

Analyzing Effect of View Factors on Surface Heat Flux, Surface Temperature, and Vegetation Cover

NALAN DEMIRCOGLU YILDIZ (✉ nalandemircioglu25@hotmail.com)
Ataturk University: Ataturk Universitesi <https://orcid.org/0000-0002-4871-1579>

Firat Erdem

Eskişehir Technical University: Eskisehir Teknik Universitesi

Seyma Berk Acet

Eskişehir Technical University: Eskisehir Teknik Universitesi

Ugur Avdan

Eskişehir Technical University: Eskisehir Teknik Universitesi

Research Article

Keywords: Urban, Surface heat flux (SHF), Sky view factor(SVF), Land surface temperature (LST), NDVI

Posted Date: April 20th, 2022

DOI: <https://doi.org/10.21203/rs.3.rs-1449162/v1>

License:  This work is licensed under a Creative Commons Attribution 4.0 International License. [Read Full License](#)

Version of Record: A version of this preprint was published at Environmental Science and Pollution Research on January 21st, 2023. See the published version at <https://doi.org/10.1007/s11356-023-25261-9>.

Abstract

With the increase in population in cities, economic, social and environmental problems continue to increase, and it is thought that the microclimatic conditions created by these problems will cause more environmental problems. One of the factors affecting the urban climate in urban areas is urban geometry. The climate of a region changes due to the shape of the land surface, human activities, atmospheric movements, and latent and sensible heat fluxes. Sky View Factor (SVF), Building View Factor (BVF) and Tree View Factor (TVF) are actively used in the determination of urban geometry. However, studies on how these factors affect the thermal state of the urban environment are insufficient. Determining the land surface changes and thermal condition characteristics (LST, NDVI, SHF and LHF) depending on urban growth and examining how these properties affect thermal conditions is very important in the construction of sustainable urban planning. In the study, SVF, BVF, TVF, LST, NDVI, SHF and LHF values of 55 points determined for three different areas with different urban geometries were calculated. How these values affect each other and their situation on urban outdoor thermal comfort is evaluated. In the study, statistical analysis was performed to evaluate the relationship between surface temperature, surface heat fluxes, different view factors, and vegetation. As a result of ANOVA analysis, it was determined as very significant ($p > 0.01$) in all regions. Both SHF and LHF values differ with SVF. The SHF value has a direct relationship with the SVF value. LHF is inversely proportional to the SVF value. The situation is reversed for SHF variation concerning vegetation. LHF and NDVI are directly related. SHF and NDVI are inversely proportional. SVF and NDVI values also vary according to the LST value. It has been observed that LST has a direct relationship with SVF and an inverse relationship with NDVI.

Introduction

The number of people living in the world is increasing day by day. It is estimated that this number will be higher in the coming years, especially in underdeveloped countries and urban centers. With the increase in population, economic, social, and environmental problems continue to increase. It is thought that the microclimatic conditions created by these problems will cause more environmental problems, especially in cities. The climate of a city is connected with processes such as man-made changes, physical characteristics of the city, latent and sensible heat fluxes, and changes in the atmosphere (Harde 2017). The biggest of the microclimatic problems is the urban heat island problem seen in cities (Nakata and Souza 2013; Allegrini et al. 2015). With urbanization, the energy distribution in the area changes with the increase of impervious surfaces. This causes the surface temperature (LST) of urban areas to be significantly higher than the surrounding rural areas. This difference is termed the Urban Heat Island (UHI) (Connors et al. 2013; Liu and Zhang 2011; Imhoff et al. 2010).

Impervious surfaces such as buildings and asphalt surfaces in urban areas collect heat during the day, next they release the heat at night (Roth and Chow 2012; Zhao et al. 2014; Brager and Dear 1998; Saito et al. 1990). This temperature change occurs not only between urban and rural areas but also in parts of the city with varying land surface. Changing surface properties also cause changes in surface heat flux (Offerle et al. 2006; Solecki et al. 2005). The reason for the change in surface heat flux may be due to the differences in the material used on the surfaces, the height of the building, the width of the street, the spaces between the buildings, the amount of green space per unit, weather conditions and socio-economic activities (Middel et al. 2014; Stewart and Oke 2012; Hamdi and Schayes 2007; Unger 2004; Johansson and Emmanuel 2006). The physical structure of residential areas affects the temperature distribution of the region, solar radiation, air quality, and wind flow as well as the local climate (Feizizadeh and Blaschke 2013; Lindberg et al. 2008; Lai and Cheng 2009; Unger 2009; Weng and Yang 2006).

The urban geometry is one of the urban environmental elements that contribute greatly to the heightened thermal condition of the urban region. Buildings obstruct clear skies and cause the area to cool more slowly at night (Oke 1981). Three key elements of urban outdoor environments are street view factors (VFs) for the sky, trees, and buildings. Although many methods are used to find these parameters, Google Street View (GSV) images have been increasingly used in recent years. Carrasco-Hernandez et al. (2015) is the team that carried out the first study to determine the Sky View Factor (SVF) from the GSV. Gong et al. (2018), on the other hand, extended the sky view factor derived from GSV to include the tree view factor (TVF) and building view factor (BVF). Radiative energy transfer, which plays a vital role in urban thermal conditions, is used to define the geometric interaction between distinct urban street components. The geometric ratio of the hemisphere supported by a horizontal surface of the amount of sky, trees, and buildings are seen are defined as SVF, TVF, and BVF, respectively (Johnson and Watson 1984).

SVF, which is one of the view factors used to characterize urban geometry, is a widely used indicator of urban geometry since it indicates how much sky is obscured at a certain place (Watson and Johnson 1987). Various urban climate studies, such as the research of urban heat islands, have used the sky view factor (Wang and Akbari, 2014). SVF is a critical geometric criterion for urban microclimate (Johansson, 2006; Bourbia and Boucheriba, 2010), urban heat island (UHI) effect (Oke 1981; Unger 2004), urban thermal comfort (Krüger et al. 2011) studies. SVF has a typical influence on the urban thermal environment in the form of a shift in radiant effect. The variation of the SVF value in different locations and the differentiation of the radiation effect cause a change in the energy budget within the area. Higher Sky View Factor locations are projected to cool faster as a result of buildings obstructing a larger amount of the sky barrier, resulting in lower levels of longwave radiation retention within the urban canopy layer (Gal et al. 2009; Daramola and Balogun 2019). The contribution of the street tree canopy to lowering

urban temperature has an ecological service role in reducing UHI, as assessed by TVF (Li and Norford 2016). Tree shadowing reduces radiation reaching ground level and evaporative cooling from leaf surfaces, resulting in a cooling effect (Shashua-Bar and Hoffman 2002). The BVF can be used to measure the impact of buildings on the urban radiation balance. Many urban building materials have a high heat capacity and thermal acceptance on the surface. This enables them to efficiently absorb and hold heat during the day and release it at night, resulting in a high UHI effect (Roth and Chow 2012).

SVF is a set of structures and trees that influence air temperature (Hien and Kardinal 2010). By giving shade to the environment, street trees minimize SVF, resulting in a less net longwave loss at night (Oke 1989). In comparison to cool skies and trees, buildings generate more long-wave radiation. As a result, urban street canyons with a higher BVF will generate more net longwave radiation. The different land uses of urban areas also affect the surface temperature (LST). Green areas, in particular, reduce the temperature in the urban environment (Kuang et al. 2015). Vegetation generally has a lower surface temperature because it has higher evaporation and emissions than built-up areas (Hamada and Ohta 2010). Some studies in the literature examines the relationship between LST and green spaces (Chen et al. 2006; Voogt and Oke 2003; Weng et al. 2004).

Reduced evaporative heat flux, as well as shortwave and longwave radiation trapping, characterize the urban climate (Oke 2002). The thermal environment is an expression of energy balance and a basic component of the eco-environment (Weng 2009). Heat loss through convection and conduction is referred to as sensible heat flux (SHF). The main source of warming in the atmosphere is known as heat loss. The heat loss from the surface due to evapotranspiration is known as latent heat flux (LHF). The sum of SHF and LHF values is defined as usable energy. Differences in land surfaces in cities also create differences in heat fluxes (Offerle et al. 2006). Therefore, understanding the variety of different surface features and land uses of a city is important in understanding the thermal state of the urban environment. Past research has focused only on the effects of land use differences on surface thermal conditions. Understanding the geometric structure of the city, the heterogeneity of the city surface, and the relationship between urban climate is still incomplete. However, it is critical to examine the impact of the thermal state of urban areas on the urban environment. Therefore, in this study, the building composition and structure of the urban environment and its associated thermal state were determined. By determining the view factor over the selected locations in the city, the land surface temperature, the presence of vegetation, and the surface temperature flux of these areas were evaluated.

Material And Methods

2.1. Material

The study area has been located in Istanbul which is the most populated province of Turkey. Considering the rapid growth of the population in recent years, very high buildings have been built. Due to the rapid expansion of the city, construction often moves out of the city. Istanbul has a climate that is a mix of Mediterranean, humid subtropical, and oceanic. It has cool winters with regular precipitation and warm to hot (mean temperatures rising at 20°C to 25°C in August, depending on location) summers with relatively dry weather. The weather in the spring and fall is normally warm, with variable conditions depending on the direction of the wind.

The study area has been determined within the borders of Istanbul. This study area includes high-rise buildings (Zone 1), dense buildings (Zone 2), and a mix of green space and buildings (Zone 3). The locations of the study area and points where the fisheye images were collected have been given in Figure-1.

In this study, Landsat-8 OLI/TIRS satellite images have been used to produce sensible heat flux, latent heat flux, LST, and NDVI maps. The images for path 180 and row 31 for 2nd August 2020 and 5th October 2020 have been acquired from the Earth Explorer portal of the United States Geological Survey (USGS). Images have been cloud-free for the study area. In addition to the Landsat-8 images, meteorological data have been used to produce the sensible heat flux. These data have included hourly air temperature, relative humidity, precipitation, solar radiation, wind speed, and, acquired from the meteorological observation station near the study area.

2.2. Methods

The method of the study can be divided into three parts. In the first part of the study sky view factor, building view factor and tree view factor parameters have been calculated. In the second part of the study sensible heat flux, latent heat flux, land surface temperature, and NDVI maps have been produced. Statistical analysis has been carried out in the last part of the study. A flowchart of the study has been given in Figure-2.

2.2.1. View Factors (SVF- BVF- TVF)

Sky View Factor (SVF), demonstrates the ratio of sky hemisphere visible from the ground (Bernard, et al. 2018). As a result of calculating SVF, a value between 0 and 1 is obtained. SVF values close to 0 represent obstructed space and values close to 1 represent open spaces (Mojolaoluwa, et al. 2019). Calculating the building view factor (BVF) and tree view factor (TVF) is similar to SVF but represents the geometric ratio of the amount of the buildings and trees, respectively, rather than the sky.

In this study, SVF, BVF, and TVF have been calculated using the GSV2SVF tool (Liang, et al. 2020) for each sampling point. GSV2SVF uses Google Street View (GSV) panoramas in Google Maps to interactively calculate sky, building, and tree view factor parameters (Fig. 3). In GSV2SVF, a GSV panorama is classified pixel-based into the sky, tree, and building classes, and then transformed into a fisheye image. Ratios of the sky, building, and tree pixels in the classified fisheye image are used for producing view factors (Liang, et al. 2020).

2.2.1. View Factors (SVF- BVF- TVF)

Relevant changes in heat flux intensities exist within cities due to the heterogeneity of the land surface, a trait that is significant because of the effect it has on the local climate (Daramola and Balogun 2019). Therefore, it is very important to examine the surface heat flux variation for the thermal conditioning of an urban environment. Available energy is generally known as the sum of sensible heat flux and latent heat flux components. The heat lost to the air due to convection and conduction is expressed as sensible heat flux. On the other hand, the heat loss from the surface as a result of evapotranspiration is expressed as latent heat flux. In this study, both sensible heat flux and latent heat flux parameters were examined to reveal the surface heat flux variation (Daramola and Balogun 2019).

In this study, sensible heat flux and latent heat flux maps have been produced by using the METRIC model (Allen et al., 2007) in the "water" package (Olmedo, et al. 2016) in the R platform. METRIC is an algorithm for calculating surface energy balance (1).

$$LE = R_n - G - H$$

1

where LE is latent heat flux consumed by ET_a ($W \cdot m^{-2}$); R_n is net radiation ($W \cdot m^{-2}$); G is soil heat flux ($W \cdot m^{-2}$), and H is the sensible heat flux convected to the air ($W \cdot m^{-2}$) (Olmedo et al. 2016).

In the METRIC model, R_n is calculated by subtracting all incoming radiant fluxes from all outgoing radiant fluxes, and it takes into account both solar and thermal radiation (2) (Allen et al. 2007). G has been calculated using (3) which considers R_n , surface temperature (T_S), normalized difference vegetation index (NDVI), and albedo (α) (Olmedo et al. 2016).

$$R_n = R_{S\downarrow} - \alpha R_{S\downarrow} + R_{L\downarrow} - R_{L\uparrow} - (1 - \epsilon_0) R_{L\downarrow}$$

2

$$\frac{G}{R_n} = (T_S - 273.15) (0.0038 + 0.0074\alpha) (1 - 0.98NDVI^4)$$

3

where $R_{S\downarrow}$ is incoming short-wave radiation ($W \cdot m^{-2}$); α is surface albedo; $R_{L\downarrow}$ is incoming long-wave radiation ($W \cdot m^{-2}$); $R_{L\uparrow}$ is outgoing long-wave radiation ($W \cdot m^{-2}$); $(1 - \epsilon_0) R_{L\downarrow}$ is the fraction of incoming long-wave radiation reflected from the surface.

NDVI has been calculated using (4). The surface temperature has been calculated using (5) based on the Split Window algorithm (Jimenez-Munoz et al. 2014).

$$NDVI = \frac{NIR - RED}{NIR + RED}$$

4

$$T_S = T_{10} + 1.378(T_{10} - T_{11}) + 0.183(T_{10} - T_{11})^2 - 0.268 + (54.30 - 2.238\omega)(1 - \epsilon) + (-129.20 + 16.40\omega)\Delta\epsilon$$

5

where T_{10} and T_{11} are the at-sensor brightness temperatures for bands 10 and 11 of Landsat-8 OLI image, ϵ is the mean emissivity, ω is the total atmospheric water vapor content ($g \cdot cm^{-2}$) and $\Delta\epsilon$ is the emissivity difference.

Pixels with near extreme conditions (hot and cold anchor pixels) have been selected for calculating the H. After selecting anchor pixels, H has been calculated using (6)

$$H = \frac{\rho \cdot c_p \cdot dT}{r_{ah}}$$

6

where dT is the difference between land surface temperature and near-surface temperature, r_{ah} is the aerodynamic resistance to heat transport ($s \cdot m^{-1}$), ρ is the air density ($kg \cdot m^{-3}$) and c_p is the specific heat of the air ($J \cdot kg^{-1} \cdot K^{-1}$). dT is solved using the linear relationship between air temperature and the estimated surface temperature of the anchor pixels. Using an iterative correction procedure based on the Monin-Obukhov equations, wind speed is projected to a height where buoyancy and mechanical mix forces are equal to compute r_{ah} (Olmedo et al. 2016).

Results

In urban climate studies, many factors such as the morphological structure of the city, the presence of green areas, and material diversity are examined and analyzed to reveal the climate structure of the city.

View factor values are a dimensionless scale ranging from 0 to 1 that is used to describe sky clarity in natural terrain and built-up areas. Three key visual indicators of the urban outdoor environment are SVF, TVF, and BVF. This study aims to determine the effects of these factors on the temperature of the city by determining the Sky View Factor (SVF), Building View Factor (BVF), Tree View Factor (TVF) of urban environments with different characteristics, using Google Street View (GSV). As a result, SVF, TVF, and BVF maps were created to understand the morphology of the city.

In the study area, three different settlements with dense buildings and green areas (Zone 1), low heights but high residential density (Zone 2), and high-rise buildings (Zone 3) were determined, and 55 random points were assigned to these areas. The building height map of the study area is given in Figure 4. While the heights of the buildings in the 1st and 2nd zones are 4 m, the heights of the buildings in the 3rd zone exceed 16 m.

3.1. Determination of SVF values

The SVF values of these areas were determined for August. A value of 0 represents the points where the sky is slightly visible, and the value of 1 represents the points where the sky is completely visible.

The results were exported to Excel for statistical analysis. In general, SVF in Zone 1 ranges between 0.20 and 0.80. In Zone 2, this value is between 0.31-0.70. On the other hand, in Zone 3, the SVF value is between 0.10-0.70. When all residential areas were evaluated, the average SVF value was found to be 0.52 in Zone 1, 0.53 in Zone 2, and 0.43 in Zone 3 (Figure-5).

The SVF values accurately depict the significant disparities between low-rise and high-rise buildings, as well as the transition between them.

3.2. Determination of BVF values

In the study, the BVF values of the points were determined to determine the effect of the buildings on the urban radiation balance. BVF values vary between 0-0.75 in Zone 1, 0.24-0.67 in Zone 2, and 0.45-0.49 in Zone 3. The averages were found to be 0.21-0.30-0.27, respectively (Figure-6).

3.3. Determination of TVF values

In the study, TVF values were determined to determine the effect of buildings on urban radiation balance. It varies between 0-0.79 in Zone 1, 0.02-0.67 in Zone 2, and 0.04-0.49 in Zone 3. The averages were found to be 0.21-0.30-0.27, respectively (Figure-7).

3.4. Determination of LST values

In this study, the Land Surface Temperature (LST) map, which is one of the indicators of urban land transformation, is shown in Figure-8. LST distribution was highest in Zone 2 ($42.7^{\circ}C$) and lowest in Zone 3 ($36.3^{\circ}C$). When the LST data were evaluated, the mean temperature values of these areas were found to be $38.6^{\circ}C$ in Zone 1, $40.8^{\circ}C$ in Zone 2, and $37.8^{\circ}C$ in Zone 3. It has been determined that the temperature density decreases from the region of maximum intensity to the region of minimum intensity.

3.5. Determination of NDVI values

The Normalized Difference Vegetation Index (NDVI) indicates the extent of vegetation in the area. When the NDVI distribution and data were evaluated, the values for these areas were found to be 0.19 in Zone 1, 0.12 in Zone 2, and 0.11 in Zone 3. The maximum NDVI values in the zones were 0.32, 0.25, and 0.26, respectively (Figure-9).

3.5. Determination of SHF values

The surface heat flux (SHF) distribution within the study area is shown in Figure-10. It has been observed that the least felt heat flux is 332.05 W/m^2 . This value was determined in Zone 3. The highest value was found in Zone 2 with 496.94 W/m^2 .

3.6. Determination of LHF values

The latent heat flow distribution (LHF) (Figure-11) was found to be the lowest in Zone-2 with 21.92 W/m^2 and the highest in Zone-3 with 220.16 W/m^2 .

When Zone 1 was evaluated, the mean value of SVF was 0.80, the TVF value was 0.79, and the BVF value was 0.75. LST value was determined as a minimum temperature of 36.3°C , a maximum temperature of 39.9°C , and an average temperature of 38.3°C . The average LHF value is 117.50 and the SHF value is 484.6. The NDVI value was found to be 0.22 at the highest and 0.07 at the lowest. When Zone 2 was evaluated, the mean value of SVF was 0.53, the TVF value was 0.14, and the BVF value was 0.30. LST value was determined as a minimum temperature of 39.2°C , a maximum temperature of 42.7°C , and an average LST value of 40.8°C . The average LH value is 72.2, and the SH value is 429.4. The NDVI value was determined as 0.16 at the highest and 0.05 at the lowest. When Zone 3 was evaluated, the mean value of SVF was 0.43, the TVF value was 0.25, BVF value was 0.27. LST value was determined as a minimum temperature of 36.3°C , a maximum temperature of 39.9°C , and an average temperature of 37.8°C . The average LHF value is 128.9 and the SHF value is 381.8. The highest NDVI value was 0.16 and the lowest 0.02 (Table-1).

Discussion

The climate of a region changes with the reasons such as the shape of the land surface, human activities, atmospheric movements, and latent and sensible heat movements. Reasons such as urbanization, increase in human activities and socio-economic development of the region cause an increase in surface temperature. (Daramola ve ark., 2018). In summer, the climate of big cities causes thermal discomfort and reduces the quality of life. Buildings and urban areas with impervious surfaces covered with asphalt surfaces store heat during the day and release it at night. This in turn affects the energy distribution and causes a temperature concentration called an urban heat island. The UHI effect reasoned by human thermal comfort, air pollution and climate and urban morphologies creates planning concerns in cities. Urban radiation balance and thermal environment are significantly affected by the geometry of cities. (Ooka ve ark, 2011). This change is not only between the rural area and the urban area but also within the urban area itself. This difference within the urban area is greater in areas with changing land surfaces. The change of the land surface properties significantly affects the surface heat flux. For example, factors that make up the physical structure of the city, such as building heights, spaces between buildings, street width, in other words, urban geometry, affect the climate of the city as it affects the temperature distribution of the region, the flow of the wind, and the air quality (Chen ve ark. 2012; Middel ve ark. 2014). Buildings block the clear sky, affecting the cooling of the area at night. SVF, BVF, and TVF values are actively used in the determination of urban geometry. However, studies on how these factors affect the thermal state of the urban environment are insufficient. It is very important to determine the changes in the land surface as a result of urbanization and the surface thermal condition characteristics (LST, NDVI, SHF, and LHF) and to know how these characteristics affect the thermal conditions in the construction of sustainable urban planning. The association between air temperature and SVF has been studied in a number of ways. Oke et al (1991) demonstrated that a difference in SVF between the suburbs and the city might result in a temperature differential of $5-7^\circ\text{C}$. Yamashita et al (1986) discovered a strong association between air temperature and SVF in 1986. Karlsson (2000) proposed a link between air temperature, pure sun energy, and SVF in forests. Svensson(2004) demonstrated that air temperature overnight and SVF have a substantial relationship, and that both land use and SVF influence air temperature changes in urban areas. However, Eliasson (1996) and Barring et al. (1985) showed that there is no statistical relationship between the geometry of urban straits and air temperature. According to Blankenstein and Kuttler (2004), SVF cannot characterize thermal qualities, the variety inside the urban heat island cannot be anticipated only by SVF.

The study calculated SVF, BVF, TVF, LST, NDVI, SHF, and LHF values of 55 points determined in three different areas with different urban geometries. How these values affect each other and their situation on urban outdoor thermal comfort is evaluated. According to the study, the highest SVF value was determined in the 1st and 2nd regions (0.53) where the buildings and trees are located. The reason why this value is low in Zone 3 where there are high-rise buildings is the distance between the buildings. However, the BVF value reaches its maximum values in Zone 3 (0.75) as expected (Figure-12). As expected, NDVI (0.22) and TVF (0.80) values are higher in Zone-1, where green areas are present compared to other regions.

The sky view factor (SVF), tree view factor (TVF), and building view factor (BVF) represent the hemispherical ratio calculated by the sky, trees, and buildings when viewed from a location, respectively. To balance urban radiation, these three view factors interact with one another. SVF is a set of structures and trees that influence air temperature. SVF is decreased by street trees because they provide shade to the environment, resulting in less net longwave loss at night. In comparison to cool skies and trees, buildings generate more long-wave radiation. As a result, urban street canyons with a higher BVF will generate more net longwave radiation. The street tree canopy as measured by the TVF serves ecologically because it reduces the urban temperature. The cooling effect of trees occurs due to the cooling of the radiation reaching the ground surface by evaporation from the leaf surfaces and the shadow effect of the trees. The buildings in the study areas have different heights and material variety. This causes buildings to have a higher heat capacity and surface heat compared to other areas. An Urban Heat Island is formed when buildings retain heat during the day and release it at night (UHI).

The view factors caused by urban geometry differ with their contribution to thermal conditions (Mirzaei and Haghigat, 2010). Therefore, this study, it is aimed to determine the effects of changes in land surface properties due to urban growth on the surface thermal condition, especially LST. As a result of the study, it was found that the surface heat flux and surface temperature change in regions with different urban geometries.

Cheung et al. (2016) determined in their study that the lower the sky visibility factor, the greater the effect on the thermal state of an area. Gal et al. (2009), Hungary (Szeged), in their study, found that areas with higher SVF values cooled faster. With their study, they confirmed the thesis of Unger (2009), who argued that urban geometry affects urban climate. It is also known that urban geometry can affect nighttime thermal conditions (Svensson, 2004). Studies have found a link between land surface temperature and sky view factor (SVF) levels ranging from moderate to high (LST)(Kim et al. 2022).

When the correlation of surface heat fluxes with LST was evaluated, the effect degrees of each factor were found to be significant ($p < 0.01$). NDVI factor affects surface flow values and LST more than SVF. The SVF value varies between 0.1 and 0.8. While this value is between 0.2 and 0.8 in 1 region, this value is between 0.1 and 0.71 in 3 regions. Svensson (2004) emphasized in his studies that the SVF value has low values (below 0.5) of the sky visibility factors in places where the density of the urban tissue is high. Low-rise buildings and green areas in 3 regions confirm this view with an average of 0.4. The average SVF value in the 1st Region, where high-rise buildings are located, is 0.53.

The SHF value represents heat loss in the air due to convection and conduction, which is the primary driver of global warming. In contrast, LHF refers to heat loss from the surface as a result of evapotranspiration. The sum of the two components is known as usable energy. Differences in the land surface in urban areas also create differences in heat flow densities. It is important to identify these differences in heat flux as they affect the thermal state of the urban environment. It has been observed that the perceived heat flux is above 300 W/m^2 . The average SHF value in Zone 1 was 434.76 W/m^2 , in Zone 2 it was 429.46 W/m^2 , and in Zone 3 it was 381.89 W/m^2 . LHF distribution, on the other hand, is in the area with the highest SHF heat flux density, with the lowest average value of 117.51 W/m^2 (Figure-13).

As a result of the study, it was found that the surface features of urban areas cause an increase in heat flux and surface temperature densities. Cities are spreading from the city center to their surroundings (Balogun et al. 2011). Ogunjobi et al. (2018) stated that in urban centers with high urban density and high-rise buildings, surface energy forms also change as surface conditions change. Jiang et al. (2014) and Guo and Schuepp (1994) stated that surface heat flux and surface temperature density also depend on the heterogeneity of urbanization. The decrease in the vegetation cover and the increase in the impermeable surface cover change the SHF and LHF densities. These two factors are very important in heat flux variation (Brom et al. 2009).

SHF value was found to be more intense on impermeable surfaces in urban areas and LHF value was found more intense in green areas. Daramola and Balagun (2019) reached the same conclusion in their study. This explains the high SHF heat value in areas with high-rise buildings. Dense structures consist of materials with high thermal storage capacity and prefer sensing heat flux over locations. On the other hand, green areas have higher LHF density compared to the city center. The high SHF density over the city center has an impact on the thermal state of the urban environment as it contributes significantly to the urban heat island effect.

The two indicators of urban land regeneration used in this study are Land Surface Temperature (LST) and Normalized Difference Vegetation Index (NDVI). The LST distribution was highest in Zone 2 (40.9°C), that is, in the densely populated urban area. The lowest intensity (37.9°C) was observed in Zone 3, where high-rise buildings are located. The Normalized Difference Vegetation Index (NDVI) indicates the extent of vegetation in the area. The level of land conversion within the city is also shown by the NDVI value. The highest NDVI values ranging from 0.07 to 0.22 were observed in Zone 1. As the degree of transformation from vegetated surface to urban surface increases, the NDVI value decreases. This explains why the maximum LST values in regions with the lowest NDVI values (Figure-14).

When the values in the study areas are processed on 3D maps, the spatial differences are more clearly understood (Figure-15).

In the study, statistical analysis was performed to evaluate the relationship between surface heat value and flow, different view factors, and vegetation. ANOVA, TUKEY, and PEARSON correlation were used to evaluate the relationship between them. The values obtained according to the ANOVA analysis (Table-2) were found to be very important ($p \leq 0.01$) in all regions. This shows how important the values revealed in the study are in determining the urban climate.

According to the results of the analysis performed to determine which values differ between regions according to the multiple comparison test, it was found that the LST value differed for all three study areas, while the SHF, TVF and SVF factors differed for one region and two or three regions. It was concluded that NDVI, LHF, and BVF values differed between one or two regions and three regions (Table-3).

According to the correlation analysis performed to determine how all values affect each other, the LST value has a very negative relationship with LHF, TVF and NDVI values, while it shows a significant positive relationship with SVF and BVF values.

The SVF value, on the other hand, has a very significant negative effect on the LHF, TVF, BVF values. SVF value increases as SHF and LST values increase (Table-4).

The sky view factor affects both sensible and latent heat flux in distinct ways. The sky view factor has a direct relationship with the sensible heat flow. The sky view factor is inversely related to the latent heat flux. In the case of surface heat flux variation about vegetation, the situation is inverted. The NDVI and latent heat flow are inextricably linked. The NDVI and the sensible heat flux are inversely proportional. The temperature of the land surface varies as well, depending on the Sky View Factor and the vegetation. LST has a direct association with the Sky View Factor and an inverse relationship with vegetation, according to research.

The lowest LST (37.8 0C) and SHF (381.89) values in the study areas were observed in the 3rd region where NDVI values are high and vegetation is present. It reduces the surface temperature and SHF density due to the evaporative cooling effect of green areas; however, with the increase in vegetation, the LHF density increases. Similar observations were found in Akure, Nigeria, in areas with high SHF and LST values, high SVF, and Low NDVI values (Daramola and Balagun 2019). According to Sahana et al. (2016), in the Sundarban Biosphere Reserve in India, Sannigrahi et al. (2017) found that green areas have low LST in their study at the Hyderabad Municipal Corporation, Anyanwu and Kanu (2006), Hamada and Ohta (2010) and Adeyeri et al. (2016) emphasized that vegetation decreases both surface and air temperatures by evaporation, which in turn cools the surface. Tan et al. (2016) emphasized that the cooling effects of urban trees are highly correlated with SVF. Tan et al. (2017) determined that the temperature values measured under the trees decreased due to the decrease in SVF values.

Conclusion

The study showed that the surface properties of the urban environment also cause an increase in heat flux and surface temperature densities. It was determined that the sky visibility factors that characterize the urban geometry also affect the surface heat flow and surface temperature. Different visibility characteristics were tested in various regions of the city, particularly areas caused by structures and buildings in the urban environment. The thermal conditions of the urban environment are influenced by the combined effect of urban geometry and surface features. As a result of these circumstances, the temperature in the city skyrockets. In cities, this results in the UHI effect. Paying heed to the findings of the urban planning study is considered a significant result.

Declarations

Data availability

Supplementary data to this article will be provided on request.

Author information

Atatürk University Faculty of Architecture and Design, Department of Landscape Architecture, Erzurum, nalandemircioglu25@hotmail.com-yildiz@atauni.edu.tr, 0000-0002-4871-1579

Nalan Demircioglu YILDIZ

Institute of Earth and Space Sciences, Eskisehir Technical University, Eskisehir, Turkey, firaterdem@eskisehir.edu.tr, 0000-0002-6163-1979

Fırat ERDEM

Eskişehir Technical University institute of graduate programs, Department of Remote Sensing and Geographic Information Systems, seymaberk@eskisehir.edu.tr 0000-0002-4366-9527

Seyma Berk ACET

Institute of Earth and Space Sciences, Eskisehir Technical University, Eskisehir, Turkey, uavdan@eskisehir.edu.tr, 0000-0001-7873-9874

Ugur AVDAN

Corresponding author

Correspondence to Nalan Demircioglu YILDIZ

Ethics declarations

Ethics approval and consent to participate

Not applicable. This article does not contain any studies with human participants or animals performed by any of the authors.

Consent for publication

Not applicable. This manuscript does not contain any studies with human participants or animals performed by any of the authors.

Competing interests

The authors declare no competing interests. This manuscript does not contain any individual person's data in any form.

Conflict of interest

The authors declare no competing interests.

Consent to Participate

Informed consent was obtained from all individual participants included in the study.

Consent to Publish

I and other writers give my consent for the publication of identifiable details, which can include a photograph(s) and/or videos and/or case history and/or details within the text ("Material") to be published in the above Journal and Article.

Authors Contributions

The idea of the original draft belongs to Nalan Demircioglu YILDIZ, Fırat ERDEM, Ugur AVDAN and Seyma Berk ACET. The introduction, literature review, and empirical outcomes sections are written by Nalan Demircioglu YILDIZ and Ugur AVDAN. Fırat ERDEM and Seyma Berk ACET constructed the methodology section in the study. All the authors read and approved the final manuscript.

Funding

The article does not have any funding

References

1. Adeyera OEA, Lawinb P, Lauxc KA, Isholad SO, Ige (2016) Analysis of climate extreme indices over the Komadugu-Yobe basin, LakeChad region: Past and future occurrences, *Weather and Climate Extremes*(23).
2. Allegrini J, Dorer V, Carmeliet J (2015) Influence of Morphologies on the Microclimate in Urban Neighbourhoods. *J Wind Eng Ind Aerodyn* 144:108–117
3. Allen RG, Tasumi M, Trezza R (2007) Satellite-based energy balance for mapping evapotranspiration with internalized calibration (METRIC) –Model. *J Irrig Drain Eng* 133(4):380–394
4. Anyanwu ECK, Kanu (2006) The role of urban forest in the protection of human environmental health in geographically-prone unpredictable hostile weather conditions, March 2006 *International journal of Environmental Science and Technology*3(2)
5. Balogun IA, Adeyewa DZ, Balogun AA, Morakinyo TE (2011) Analysis of urban expansion and land use changes in Akure, Nigeria, using remote sensing and geographic information system (GIS) techniques. *J Geogr Reg Plan* 4(9):533–541
6. Barring L, Mattsson JO, Lindqvist S (1985) Canyon geometry, street temperatures and urban heat island in Malmö, Sweden, *Journal of Climatology* 5 (1985) 433–444
7. Blankenstein S, Kuttler W (2004) Impact of street geometry on downward longwave radiation and air temperature in an urban environment. *Meteorol Z* 13:373–379
8. Bourbia F, Boucheriba F (2010) Impact of street design on urban microclimate for semi arid climate (Constantine), *Renew. Energy*, 35 (2) (Feb. 2010), pp. 343–347
9. Brager GS, de Dear RJ (1998) Thermal adaptation in the built environment: a literature review, *Energy Build.*, 27 (1) (Feb. 1998), pp. 83–96
10. Brom J, Prochazka J, Rejskova A (2009) Evaluation of functional properties of various types of vegetation cover using remotely sensed data analysis. *Soil Water Res* 4:S49–S58
11. Carrasco-Hernandez R, Smedley AR, Webb AR (2015) Using urban canyon geometries obtained from Google Street View for atmospheric studies: potential applications in the calculation of street level total shortwave irradiances, *Energy Build.*, 86 (2015), pp. 340–348, 10.1016/j.enbuild.2014.10.001

12. Chen L, Ng E, An X, Ren C, Lee M, Wang U, He Z (2012) Sky view factor analysis of street canyons and its implications for daytime intra-urban air temperature differentials in high-rise, high-density urban areas of Hong Kong: a GIS-based simulation approach, *Int. J. Climatol.*, 32 (1) (2012), pp. 121–136
13. Cheung HKW, Coles D, Levermore GJ (2016) Urban heat island analysis of Greater Manchester, UK using sky view factor analysis. *Build Serv Eng Technol* 37(1):5–17
14. Connors JP, Galletti CS, Chow WTL (2013) Landscape configuration and urban heat island effects: assessing the relationship between landscape characteristics and land surface temperature in Phoenix, Arizona. *Landscape Ecol* 28, 271–283 (2013). <https://doi.org/10.1007/s10980-012-9833-1>
15. Daramola MT, Eresanya EO, Ishola KA (2018) Assessment of the thermal response of variations in land surface around an urban area, *Model. Earth Syst. Environ.*, 4 (2) (2018), pp. 535–553, <https://doi.org/10.1007/s40808-018-0463-8>
16. Daramola MT, Balogun IA (2019) Analysis of the urban surface thermal condition based on sky-view factor and vegetation cover. *Remote Sens Applications: Soc Environ* 15:100253
17. Eliasson I (1996) Urban nocturnal temperatures, street geometry and land use. *Atmos Environ* 30:379–392
18. Erell E, Williamson T (2007) Intra-urban differences in canopy layer air temperature at a mid-latitude city, *Int. J. Climatol.*, 27 (2007), pp. 1243–1255
19. Feizizadeh B, Blaschke T (2013) Land Suitability Analysis for Tabriz County, Iran: A Multi-Criteria Evaluation Approach Using GIS. *J Environ Plann Manage* 56:1–23
20. Gal T, Lindberg F, Unger J (2009) Computing continuous sky view factors using 3D urban raster and vector databases: comparison and application to urban climate, *Theor. Appl. Climatol.*, 95 (2009), pp. 111–123
21. Gong FY, Zeng ZC, Zhang F, Li X, Ng E, Norford LK (2018) Mapping sky, tree, and building view factors of street canyons in a high-density urban environment, *Build. Environ.*, 134 (2018), pp. 155–167, [10.1016/j.buildenv.2018.02.042](https://doi.org/10.1016/j.buildenv.2018.02.042)
22. Guo Y, Schuepp PH (1994) On surface energy balance over the northern wetlands 1. The effects of small-scale temperature and wetness heterogeneity. *J Geophys Res Atmos* 99(D1):1601–1612
23. Hamada S, Ohta T (2010) Seasonal variations in the cooling effect of urban green areas on the surrounding urban areas. *Urban Forestry and Urban Greening* 9:15–24. doi:10.1016/j.ufug.2009.10.002
24. Hamdi R, Schayes G (2008) Sensitivity study of the urban heat island intensity to urban characteristics. *Int J Climatology: J Royal Meteorological Soc* 28(7):973–982
25. Harde H (2017) Radiation transfer calculations and assessment of global warming by CO₂. *Int. J. Atmos. Sci.* 9251034, 30. 2017. <https://doi.org/10.1155/2017/9251034>
26. Hien WN, Kardinal JS (2010) Air temperature distribution and the influence of sky view factor in a Green Singapore estate, *J. Urban Plann. Dev.*, 136 (3) (Sep. 2010), pp. 261–272
27. Imhoff ML, Zhang P, Wolfe RE, Bounoua L (2010) Remote sensing of the urban heat island effect across biomes in the continental USA. *Remote Sens Environ* 114(3):504–513. <https://doi.org/10.1016/j.rse.2009.10.008>
28. Jiang Q, Tang C, Ma E, Yuan Y, Zhang W (2014) Variations of near surface energy balance caused by land cover changes in the semiarid grassland area of China, *Adv. Meteorol.*, p.9, 894147
29. Johansson E (2006) Influence of urban geometry on outdoor thermal comfort in a hot dry climate: a study in Fez, Morocco, *Build. Environ.*, 41 (10) (Oct. 2006), pp. 1326–1338
30. Johansson E, Emmanuel R (2006) The influence of urban design on outdoor thermal comfort in the hot, humid city of Colombo, Sri Lanka, *Int. J. Biometeorol.*, 51 (2) (Nov. 2006), pp. 119–133
31. Johnson GT, Watson ID (1984) The determination of view-factors in urban canyons, *J. Clim. Appl. Meteorol.*, 23 (2) (Feb. 1984), pp. 329–335
32. Karlsson IM (2000) Nocturnal air temperature variations between forest and open areas. *J Appl Meteorol* 39:851–862
33. Kim J, Lee D, Brown RD, Kim S, Kim JH, Sung S (2002) **0. The effect of extremely low sky view factor on land surface temperatures in urban residential areas Sustainable Cities and Society Volume 80 May 2022 103799**
34. Kruger EL, Minella FO, Rasia F (2011) Impact of urban geometry on outdoor thermal comfort and air quality from field measurements in Curitiba, Brazil, *Build. Environ.*, 46 (2011), pp. 621–634
35. Kuang W, Liu Y, Dou Y, Chi W, Chen G, Gao C, Yang T, Liu J, Zhang R (2015) What are hot and what are not in an urban landscape: quantifying and explaining the land surface temperature pattern in Beijing, China, *Landsc. Ecol.*, 30 (2) (2015), pp. 357–373
36. Lai KH, Cheng TCE (2009) Just-in-Time Logistics. Gower Publishing, Farnham, England
37. Landsberg HE (1981) The Urban Climate. International Geophysics Series. Academic Press, New York

38. Li X-X, Norford LK (2016) Evaluation of cool roof and vegetations in mitigating urban heat island in a tropical city, Singapore, *Urban Clim.*, 16 (Supplement C) (Jun. 2016), pp. 59–74
39. Liang J, Gong J, Zhang J, Li Y, Wu D, Zhang G (2020) GSV2SVF-an interactive GIS tool for sky, tree and building view factor estimation from street view photographs. *Build Environ* 168:106475
40. Lindberg F, Holmer B, Thorsson S (2008) SOLWEIG 1.0—modelling spatial variations of 3D radiant fluxes and mean radiant temperature in complex urban settings, *Int. J. Biometeorol.*, 52 (7) (2008), pp. 697–713
41. Liu L, Zhang Y (2011) Remote Sens 3:1535–1552. <https://doi.org/10.3390/rs3071535>. Urban Heat Island Analysis Using the Landsat TM Data and ASTER Data: A Case Study in Hong Kong
42. Middel A, Häb K, Brazel AJ, Martin C, Guhathakurta S (2014) Impact of urban form and design on microclimate in Phoenix, AZ *Landsc, vol 122. Urban Plan*, pp 16–28
43. Mirzaei PA, Haghishat F (2010) Approaches to study urban heat island—abilities and limitations, *Build. Environ* 45:2192–2201
44. Mojolaoluwa T, Daramola, Ifeoluwa A, Balogun (2019) Analysis of the urban surface thermal condition based on sky-view factor and vegetation cover, *Remote Sensing Applications: Society and Environment*. 15:2352–9385. <https://doi.org/10.1016/j.rsase.2019.100253>
45. Nakata C, Souza L (2013) Verification of the Influence of Urban Geometry on the Nocturnal Heat Island Intensit. *J Urban Environ Eng* 7(2):286–292
46. Ng E, Yuan C, Chen L, Ren C, Fung JC (2011) Improving the wind environment in high-density cities by understanding urban morphology and surface roughness: a study in Hong Kong, *Landsc. Urban Plan.*, 101 (1) (2011), pp. 59–74
47. Offerle B, Grimmond CSB, Fortuniak K, Pawlak W (2006) Intraurban differences of surface energy fluxes in a central european city, *J. Appl. Meteorol. Climatol.*, 45 (2006), pp. 125–136
48. Ogunjobi KO, Daramola MT, Akinsanola AA (2018) Estimation of surface energy fluxes from remotely sensed data over Akure. *Nigeria Spat Inf Res* 26(1):77–89
49. Oke TR (1981) Canyon geometry and the nocturnal urban heat island: comparison of scale model and field observations, *J. Climatol.*, 1 (3) (Jul. 1981), pp. 237–254
50. Oke TR (1987) Boundary Layer Climates, Routledge (1987)
51. Oke TR (1989) The micrometeorology of the urban forest, *Phil. Trans. Roy. Soc. Lond. B*, 324 (1223) (Aug. 1989), pp. 335–349
52. Oke TR (2002) Boundary Layer Climates. Routledge, Abington-on-Thames, UK
53. Oke TR, Johnson GT, Steyn DG, Watson ID (1991) Simulation of surface urban heat islands under 'ideal' conditions at night. Part 2: diagnosis of causation. *Boundary Layer Meteorol* 56:339–358
54. Olmedo GF, Farias O, Luengo SFonseca, Fuentes Peñailillo F (2016) Water: tools and functions to estimate actual evapotranspiration using Land Surface Energy Balance Models in R. *R J 8(2):352–369*
55. Ooka R, Sato T, Harayama K, Murakami S, Kawamoto Y (2011) Thermal energy balance analysis of the tokyo metropolitan area using a mesoscale meteorological model incorporating an urban canopy model, *Bound.-Layer Meteorol.*, 138 (1) (Jan. 2011), pp. 77–97
56. Roth M, Chow WTL (2012) A historical review and assessment of urban heat island research in Singapore, *Singapore J. Trop. Geogr.*, 33 (3) (Nov. 2012), pp. 381–397
57. Sahana M, Ahmed R, Sajjad H, Model (2016) *Earth Syst. Environ.*, 2,81
58. Saito O, Ishihara T, Katayama (1990) Study of the effect of green areas on the thermal environment in an urban area, *Energy Build.*, 15 (3) (Jan. 1990), pp. 493–498
59. Sannigrahi S, Rahmat S, Chakraborti S, Bhatt S, Jha S (2017) Changing dynamics of urban biophysical composition and its impact on urban heat island intensity and thermal characteristics: the case of Hyderabad City, India. *Model Earth Syst Environ* 3(2):647–667
60. Shashua-Bar L, Hoffman ME (2002) The Green CTTC model for predicting the air temperature in small urban wooded sites, *Build. Environ.*, 37 (12) (Dec. 2002), pp. 1279–1288
61. Solecki WD, Rosenzweig C, Parshall L, Pope G, Clark M, Cox J, Wiencke M (2005) Mitigation of the heat island effect in urban New Jersey. *Glob Environ Change B* 6:30–49. doi:10.1016/j.hazards.2004.12.002
62. Stewart ID, Oke TR (2012) Local climate zones for urban temperature studies, *Bull. Am. Meteorol. Soc.*, 93 (12) (2012), pp. 1879–1900
63. Svensson MK (2004) Sky view factor analysis – implications for urban air temperature differences, *Meteorol. Appl* 11:201–211
64. Tan Z, Lau KKL, Ng E (2016) Urban tree design approaches for mitigating daytime urban heat island effects in a high-density urban environment. *Energy Build* 114:265–274
65. Tan Z, Lau KKL, Ng E (2017) Planning strategies for roadside tree planting and outdoor comfort enhancement in subtropical high-density urban areas. *Build Environ* 120:93–109

66. Unger J (2009) Connection between urban heat island and sky view factor approximated by a software tool on a 3D urban database. *Int J Environ Pollut* 36(1–3):59–80
67. Unger J (2004) Intra-urban relationship between surface geometry and urban heat island: review and new approach, *Clim. Res.*, 27 (3) (2004), pp. 253–264
68. Voogt JA, Oke TR (2003) Thermal remote sensing of urban climates. *Remote Sens Environ* 86:370–384
69. Wang Y, Akbari H (2014) Effect of sky view factor on outdoor temperature and comfort in Montreal, *Environ. Eng. Sci.*, 31 (6) (2014), pp. 272–287
70. Watson ID, Johnson GT (1987) Graphical estimation of sky view-factors in urban environments, *J. Climatol.*, 7 (2) (Mar. 1987), pp. 193–197
71. Weng Q, Lu D, Schubring J (2004) Estimation of land surface temperature–vegetation abundance relationship for urban heat island studies, *Remote Sens. Environ.*, 89 (2004), pp. 467–483
72. Weng Q (2009) Thermal infrared remote sensing for urban climate and environmental studies: methods, applications, and trends, *ISPRS J. Photogrammetry Remote Sens.*, 64 (2009), pp. 335–344
73. Weng Q, Yang S (2006) Urban Air Pollution Patterns, Land Use, and Thermal Landscape: An Examination of the Linkage Using GIS. *Environ Monit Assess* volume 117:pages463–489
74. Yamashita S, Sekine K, Shoda M, Yamashita K, Hara Y (1986) On relationships between heat island and sky view factor in the cities of Tama river basin, Japan. *Atmos Environ* 20:681–686
75. Zhao L, Lee X, Smith RB, Oleson K (2014) Strong contributions of local background climate to urban heat islands. *Nature* 511:216–219

Tables

Table-1. Parameter values of regions

ZONE 1			ZONE 2			ZONE 3			
MEAN	MIN	MAX	MEAN	MIN	MAX	MEAN	MIN	MAX	
SVF	0,52709558	0,203275	0,803103	0,53059887	0,312339	0,707306	0,43708065	0,100511	0,706928
TVF	0,2475275	0,001417	0,795007	0,14780512	0,003709	0,558815	0,25121124	0,015592	0,692356
BVF	0,2114279	0,000096	0,753528	0,30262509	0,024388	0,67213	0,27589937	0,045738	0,497792
LST	38,36583299	36,326599	39,897339	40,86010664	39,256042	42,76276	37,8734749	36,31412	39,42767
LHF	75,01897851	41,886227	117,508232	72,2419082	21,926254	134,3489	128,9560326	43,17569	220,1686
SHF	434,7602719	379,806763	484,606751	429,4596151	389,147919	496,9407	381,8921712	332,0508	491,2459
NDVI	0,12	0,07	0,22	0,09	0,05	0,16	0,08	0,02	0,16

Table-2. ANOVA values of data belonging to study areas

ANOVA		Sum of Squares	Mean Square	F	Sig.
LST	Between Groups	199,9892264	99,9946132	141,4058996	0,00
	Within Groups	80,6146415	0,7071460		
	Total	280,6038679			
LHF	Between Groups	79734,3277510	39867,1638755	56,0232234	0,00
	Within Groups	81124,5123584	711,6185295		
	Total	160858,8401094			
SHF	Between Groups	66115,3316962	33057,6658481	38,0373262	0,00
	Within Groups	99075,6785081	869,0848992		
	Total	165191,0102043			
SVF	Between Groups	0,2191880	0,1095940	6,2870238	0,00
	Within Groups	1,9872227	0,0174318		
	Total	2,2064108			
TVF	Between Groups	0,2684623	0,1342312	4,7745166	0,01
	Within Groups	3,2050056	0,0281141		
	Total	3,4734680			
BVF	Between Groups	0,1714409	0,0857205	3,3730517	0,04
	Within Groups	2,8971192	0,0254133		
	Total	3,0685601			
NDVI	Between Groups	0,0444542	0,0222234	21,776	0,00
	Within Groups	0,1155411	0,0013345		
	Total	0,1591141			

Table-3 Determining the differences of the obtained data according to the study areas

LST	<p>Tukey HSD</p> <table border="1"> <thead> <tr> <th rowspan="2">Grup</th> <th rowspan="2">N</th> <th colspan="3">Subset for alpha = 0.05</th> </tr> <tr> <th>1</th> <th>2</th> <th>3</th> </tr> </thead> <tbody> <tr> <td>Yüksek binalar</td> <td>39</td> <td>37,87347490</td> <td></td> <td></td> </tr> <tr> <td>Bina+Yeşil alan</td> <td>39</td> <td></td> <td>38,36583299</td> <td></td> </tr> <tr> <td>Yoğun binalar</td> <td>39</td> <td></td> <td></td> <td>40,86010664</td> </tr> <tr> <td>Sig.</td> <td></td> <td>1,000</td> <td>1,000</td> <td>1,000</td> </tr> </tbody> </table> <p>Means for groups in homogeneous subsets are displayed. a. Uses Harmonic Mean Sample Size = 39,000.</p>	Grup	N	Subset for alpha = 0.05			1	2	3	Yüksek binalar	39	37,87347490			Bina+Yeşil alan	39		38,36583299		Yoğun binalar	39			40,86010664	Sig.		1,000	1,000	1,000	<p>Tukey HSD</p> <table border="1"> <thead> <tr> <th rowspan="2">Grup</th> <th rowspan="2">N</th> <th colspan="3">Subset for alpha = 0.05</th> </tr> <tr> <th>1</th> <th>2</th> <th>3</th> </tr> </thead> <tbody> <tr> <td>Yüksek binalar</td> <td>39</td> <td>72,24190820</td> <td></td> <td></td> </tr> <tr> <td>Bina+Yeşil alan</td> <td>39</td> <td></td> <td>75,01897851</td> <td></td> </tr> <tr> <td>Yoğun binalar</td> <td>39</td> <td></td> <td></td> <td>128,95603259</td> </tr> <tr> <td>Sig.</td> <td></td> <td></td> <td>,890</td> <td>1,000</td> </tr> </tbody> </table> <p>Means for groups in homogeneous subsets are displayed. a. Uses Harmonic Mean Sample Size = 39,000.</p>	Grup	N	Subset for alpha = 0.05			1	2	3	Yüksek binalar	39	72,24190820			Bina+Yeşil alan	39		75,01897851		Yoğun binalar	39			128,95603259	Sig.			,890	1,000
Grup	N			Subset for alpha = 0.05																																																						
		1	2	3																																																						
Yüksek binalar	39	37,87347490																																																								
Bina+Yeşil alan	39		38,36583299																																																							
Yoğun binalar	39			40,86010664																																																						
Sig.		1,000	1,000	1,000																																																						
Grup	N	Subset for alpha = 0.05																																																								
		1	2	3																																																						
Yüksek binalar	39	72,24190820																																																								
Bina+Yeşil alan	39		75,01897851																																																							
Yoğun binalar	39			128,95603259																																																						
Sig.			,890	1,000																																																						
SHF	<p>Tukey HSD</p> <table border="1"> <thead> <tr> <th rowspan="2">Grup</th> <th rowspan="2">N</th> <th colspan="3">Subset for alpha = 0.05</th> </tr> <tr> <th>1</th> <th>2</th> <th>3</th> </tr> </thead> <tbody> <tr> <td>Yüksek binalar</td> <td>39</td> <td>381,89217122</td> <td></td> <td></td> </tr> <tr> <td>Bina+Yeşil alan</td> <td>39</td> <td></td> <td>429,45981507</td> <td></td> </tr> <tr> <td>Yoğun binalar</td> <td>39</td> <td></td> <td></td> <td>434,76027190</td> </tr> <tr> <td>Sig.</td> <td></td> <td>1,000</td> <td></td> <td>,707</td> </tr> </tbody> </table> <p>Means for groups in homogeneous subsets are displayed. a. Uses Harmonic Mean Sample Size = 39,000.</p>	Grup	N	Subset for alpha = 0.05			1	2	3	Yüksek binalar	39	381,89217122			Bina+Yeşil alan	39		429,45981507		Yoğun binalar	39			434,76027190	Sig.		1,000		,707	<p>Tukey HSD</p> <table border="1"> <thead> <tr> <th rowspan="2">Grup</th> <th rowspan="2">N</th> <th colspan="3">Subset for alpha = 0.05</th> </tr> <tr> <th>1</th> <th>2</th> <th>3</th> </tr> </thead> <tbody> <tr> <td>Yüksek binalar</td> <td>39</td> <td>,43708065</td> <td></td> <td></td> </tr> <tr> <td>Bina+Yeşil alan</td> <td>39</td> <td></td> <td>,52709558</td> <td></td> </tr> <tr> <td>Yoğun binalar</td> <td>39</td> <td></td> <td></td> <td>,53059887</td> </tr> <tr> <td>Sig.</td> <td></td> <td></td> <td>1,000</td> <td>,992</td> </tr> </tbody> </table> <p>Means for groups in homogeneous subsets are displayed. a. Uses Harmonic Mean Sample Size = 39,000.</p>	Grup	N	Subset for alpha = 0.05			1	2	3	Yüksek binalar	39	,43708065			Bina+Yeşil alan	39		,52709558		Yoğun binalar	39			,53059887	Sig.			1,000	,992
Grup	N			Subset for alpha = 0.05																																																						
		1	2	3																																																						
Yüksek binalar	39	381,89217122																																																								
Bina+Yeşil alan	39		429,45981507																																																							
Yoğun binalar	39			434,76027190																																																						
Sig.		1,000		,707																																																						
Grup	N	Subset for alpha = 0.05																																																								
		1	2	3																																																						
Yüksek binalar	39	,43708065																																																								
Bina+Yeşil alan	39		,52709558																																																							
Yoğun binalar	39			,53059887																																																						
Sig.			1,000	,992																																																						
TVF	<p>Tukey HSD</p> <table border="1"> <thead> <tr> <th rowspan="2">Grup</th> <th rowspan="2">N</th> <th colspan="3">Subset for alpha = 0.05</th> </tr> <tr> <th>1</th> <th>2</th> <th>3</th> </tr> </thead> <tbody> <tr> <td>Yüksek binalar</td> <td>39</td> <td>,14780512</td> <td></td> <td></td> </tr> <tr> <td>Bina+Yeşil alan</td> <td>39</td> <td></td> <td>,24752750</td> <td></td> </tr> <tr> <td>Yoğun binalar</td> <td>39</td> <td></td> <td></td> <td>,25121124</td> </tr> <tr> <td>Sig.</td> <td></td> <td>1,000</td> <td></td> <td>,995</td> </tr> </tbody> </table> <p>Means for groups in homogeneous subsets are displayed.</p>	Grup	N	Subset for alpha = 0.05			1	2	3	Yüksek binalar	39	,14780512			Bina+Yeşil alan	39		,24752750		Yoğun binalar	39			,25121124	Sig.		1,000		,995	<p>Tukey HSD</p> <table border="1"> <thead> <tr> <th rowspan="2">Grup</th> <th rowspan="2">N</th> <th colspan="3">Subset for alpha = 0.05</th> </tr> <tr> <th>1</th> <th>2</th> <th>3</th> </tr> </thead> <tbody> <tr> <td>Bina+Yeşil alan</td> <td>39</td> <td>,21142790</td> <td></td> <td></td> </tr> <tr> <td>Yüksek binalar</td> <td>39</td> <td></td> <td>,27589937</td> <td></td> </tr> <tr> <td>Yoğun binalar</td> <td>39</td> <td></td> <td></td> <td>,30262509</td> </tr> <tr> <td>Sig.</td> <td></td> <td></td> <td>,179</td> <td>,740</td> </tr> </tbody> </table> <p>Means for groups in homogeneous subsets are displayed. a. Uses Harmonic Mean Sample Size = 39,000.</p>	Grup	N	Subset for alpha = 0.05			1	2	3	Bina+Yeşil alan	39	,21142790			Yüksek binalar	39		,27589937		Yoğun binalar	39			,30262509	Sig.			,179	,740
Grup	N			Subset for alpha = 0.05																																																						
		1	2	3																																																						
Yüksek binalar	39	,14780512																																																								
Bina+Yeşil alan	39		,24752750																																																							
Yoğun binalar	39			,25121124																																																						
Sig.		1,000		,995																																																						
Grup	N	Subset for alpha = 0.05																																																								
		1	2	3																																																						
Bina+Yeşil alan	39	,21142790																																																								
Yüksek binalar	39		,27589937																																																							
Yoğun binalar	39			,30262509																																																						
Sig.			,179	,740																																																						
NDVI	<p>Tukey HSD</p> <table border="1"> <thead> <tr> <th rowspan="2">Grup</th> <th rowspan="2">N</th> <th colspan="3">Subset for alpha = 0.05</th> </tr> <tr> <th>1</th> <th>2</th> <th>3</th> </tr> </thead> <tbody> <tr> <td>Yüksek binalar</td> <td>39</td> <td>,07729141</td> <td></td> <td></td> </tr> <tr> <td>Yoğun binalar</td> <td>39</td> <td></td> <td>,08716816</td> <td></td> </tr> <tr> <td>Bina+Yeşil alan</td> <td>39</td> <td></td> <td></td> <td>,12248682</td> </tr> <tr> <td>Sig.</td> <td></td> <td></td> <td>,359</td> <td>1,000</td> </tr> </tbody> </table> <p>Means for groups in homogeneous subsets are displayed. a. Uses Harmonic Mean Sample Size = 39,000.</p>	Grup	N	Subset for alpha = 0.05			1	2	3	Yüksek binalar	39	,07729141			Yoğun binalar	39		,08716816		Bina+Yeşil alan	39			,12248682	Sig.			,359	1,000																													
Grup	N			Subset for alpha = 0.05																																																						
		1	2	3																																																						
Yüksek binalar	39	,07729141																																																								
Yoğun binalar	39		,08716816																																																							
Bina+Yeşil alan	39			,12248682																																																						
Sig.			,359	1,000																																																						
LST	<p>Tukey HSD</p> <table border="1"> <thead> <tr> <th rowspan="2">Grup</th> <th rowspan="2">N</th> <th colspan="3">Subset for alpha = 0.05</th> </tr> <tr> <th>1</th> <th>2</th> <th>3</th> </tr> </thead> <tbody> <tr> <td>Yüksek binalar</td> <td>39</td> <td>37,87347490</td> <td></td> <td></td> </tr> <tr> <td>Bina+Yeşil alan</td> <td>39</td> <td></td> <td>38,36583299</td> <td></td> </tr> <tr> <td>Yoğun binalar</td> <td>39</td> <td></td> <td></td> <td>40,86010664</td> </tr> <tr> <td>Sig.</td> <td></td> <td>1,000</td> <td>1,000</td> <td>1,000</td> </tr> </tbody> </table> <p>Means for groups in homogeneous subsets are displayed. a. Uses Harmonic Mean Sample Size = 39,000.</p>	Grup	N	Subset for alpha = 0.05			1	2	3	Yüksek binalar	39	37,87347490			Bina+Yeşil alan	39		38,36583299		Yoğun binalar	39			40,86010664	Sig.		1,000	1,000	1,000	<p>Tukey HSD</p> <table border="1"> <thead> <tr> <th rowspan="2">Grup</th> <th rowspan="2">N</th> <th colspan="3">Subset for alpha = 0.05</th> </tr> <tr> <th>1</th> <th>2</th> <th>3</th> </tr> </thead> <tbody> <tr> <td>Yüksek binalar</td> <td>39</td> <td>72,24190820</td> <td></td> <td></td> </tr> <tr> <td>Bina+Yeşil alan</td> <td>39</td> <td></td> <td>75,01897851</td> <td></td> </tr> <tr> <td>Yoğun binalar</td> <td>39</td> <td></td> <td></td> <td>128,95603259</td> </tr> <tr> <td>Sig.</td> <td></td> <td></td> <td>,890</td> <td>1,000</td> </tr> </tbody> </table> <p>Means for groups in homogeneous subsets are displayed. a. Uses Harmonic Mean Sample Size = 39,000.</p>	Grup	N	Subset for alpha = 0.05			1	2	3	Yüksek binalar	39	72,24190820			Bina+Yeşil alan	39		75,01897851		Yoğun binalar	39			128,95603259	Sig.			,890	1,000
Grup	N			Subset for alpha = 0.05																																																						
		1	2	3																																																						
Yüksek binalar	39	37,87347490																																																								
Bina+Yeşil alan	39		38,36583299																																																							
Yoğun binalar	39			40,86010664																																																						
Sig.		1,000	1,000	1,000																																																						
Grup	N	Subset for alpha = 0.05																																																								
		1	2	3																																																						
Yüksek binalar	39	72,24190820																																																								
Bina+Yeşil alan	39		75,01897851																																																							
Yoğun binalar	39			128,95603259																																																						
Sig.			,890	1,000																																																						

Table-4. Relation of parameter values with each other

		Correlations					
		LST	LHF	SHF	SVF	TVF	BVF
LST	Pearson Correlation	1	-,388**	,257**	,215*	-,373**	,227*
	Sig. (2-tailed)		,000	,005	,020	,000	,014
	N	117	117	117	117	117	117
LHF	Pearson Correlation	-,388**	1	-,865**	-,293**	,038	,167
	Sig. (2-tailed)	,000		,000	,001	,684	,072
	N	117	117	117	117	117	117
SHF	Pearson Correlation	,257**	-,865**	1	,254**	,092	-,274**
	Sig. (2-tailed)	,005	,000		,006	,324	,003
	N	117	117	117	117	117	117
SVF	Pearson Correlation	,215*	-,293**	,254**	1	-,460**	-,362**
	Sig. (2-tailed)	,020	,001	,006		,000	,000
	N	117	117	117	117	117	117
TVF	Pearson Correlation	-,373**	,038	,092	-,460**	1	-,656**
	Sig. (2-tailed)	,000	,684	,324	,000		,000
	N	117	117	117	117	117	117
BVF	Pearson Correlation	,227*	,167	-,274**	-,362**	-,656**	1
	Sig. (2-tailed)	,014	,072	,003	,000	,000	
	N	117	117	117	117	117	117

Figures

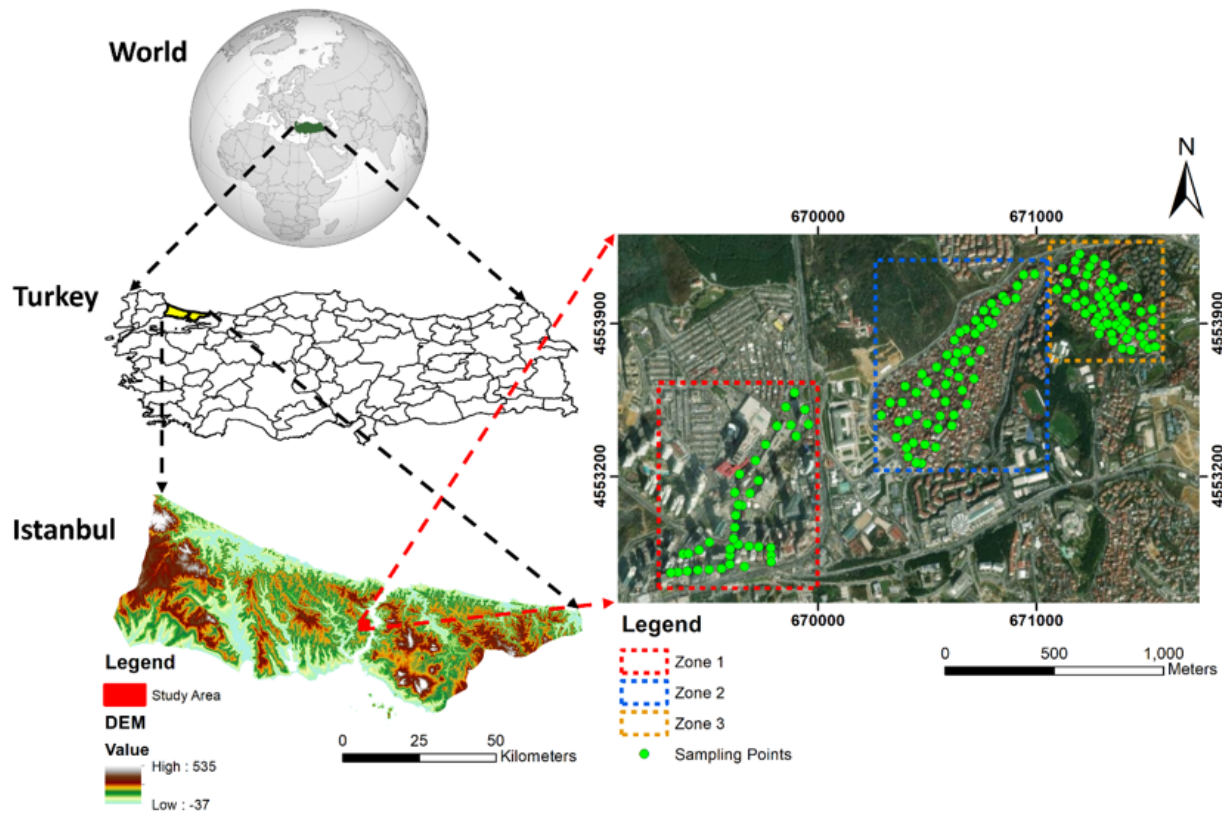


Figure 1

Study area and sampling points.

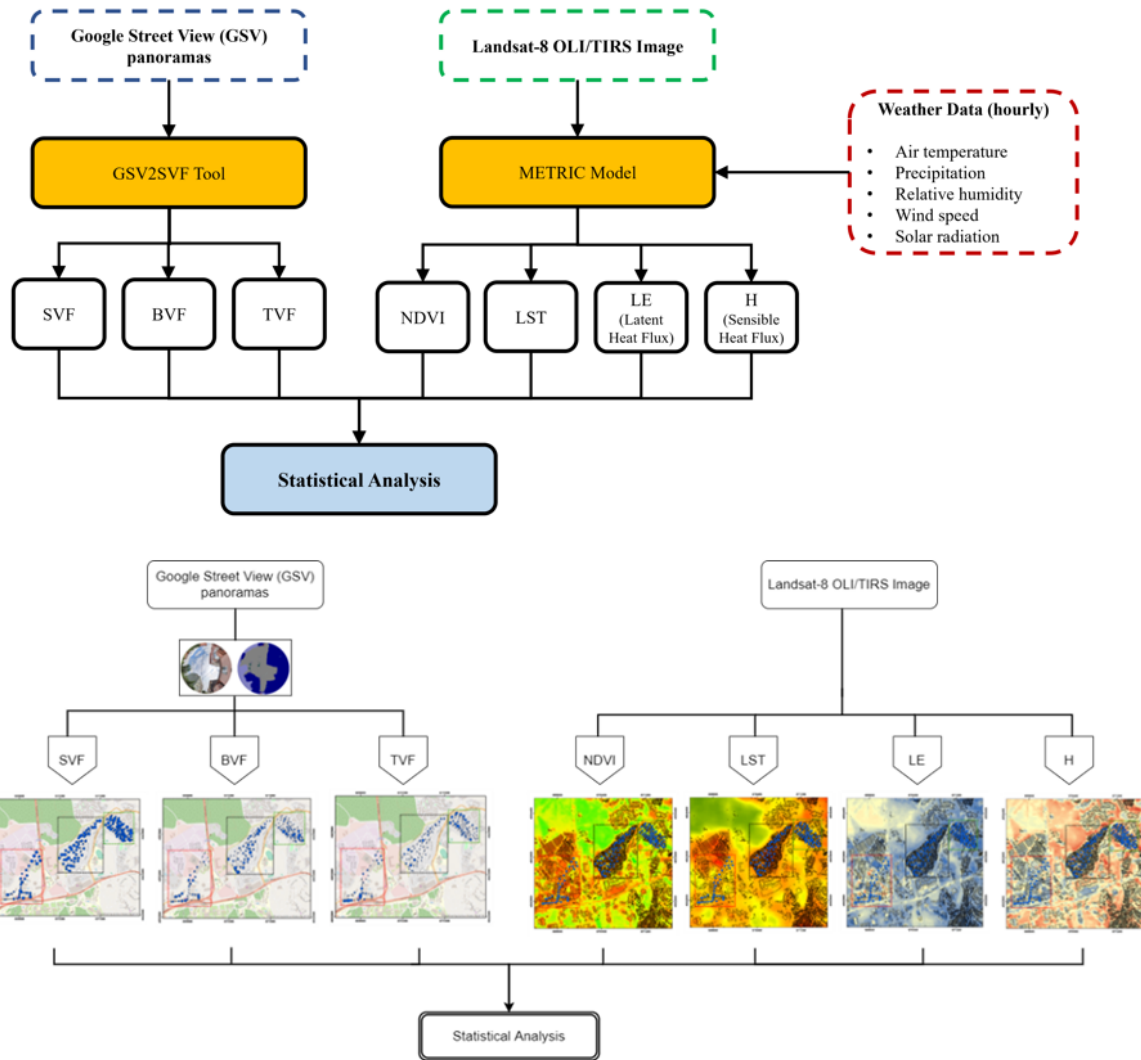


Figure 2

Flowchart of the study

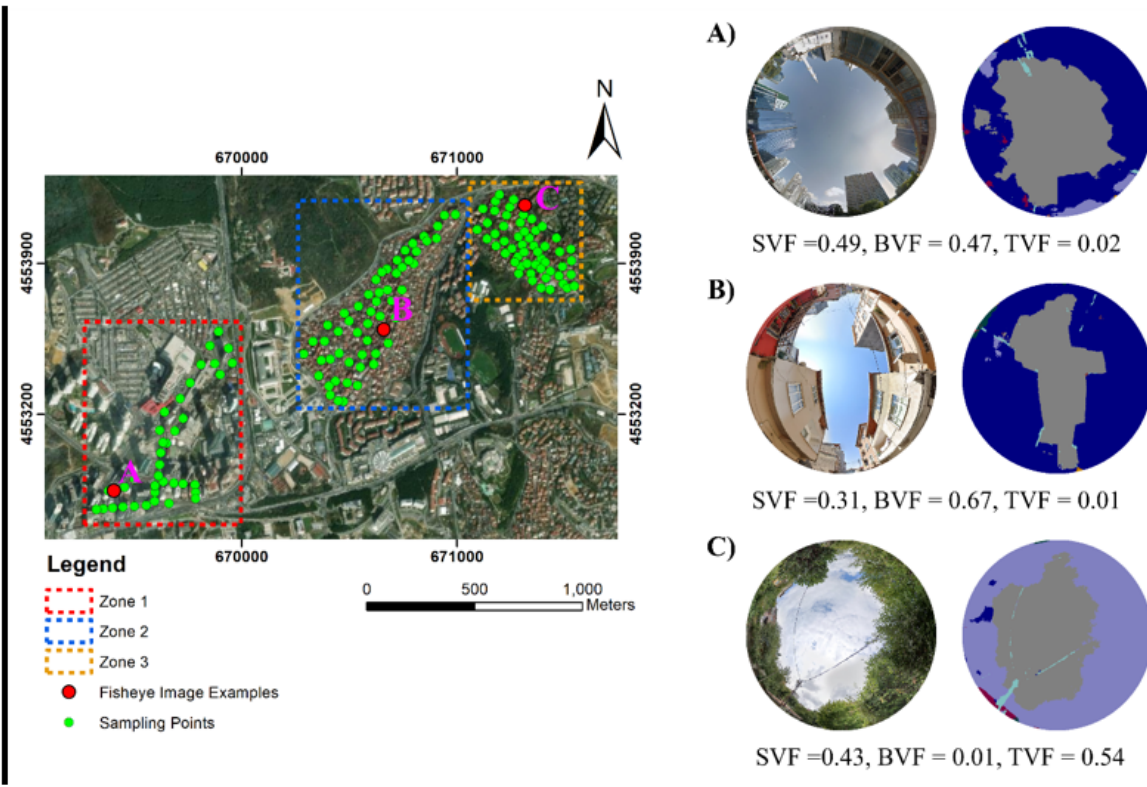


Figure 3

SVF examples

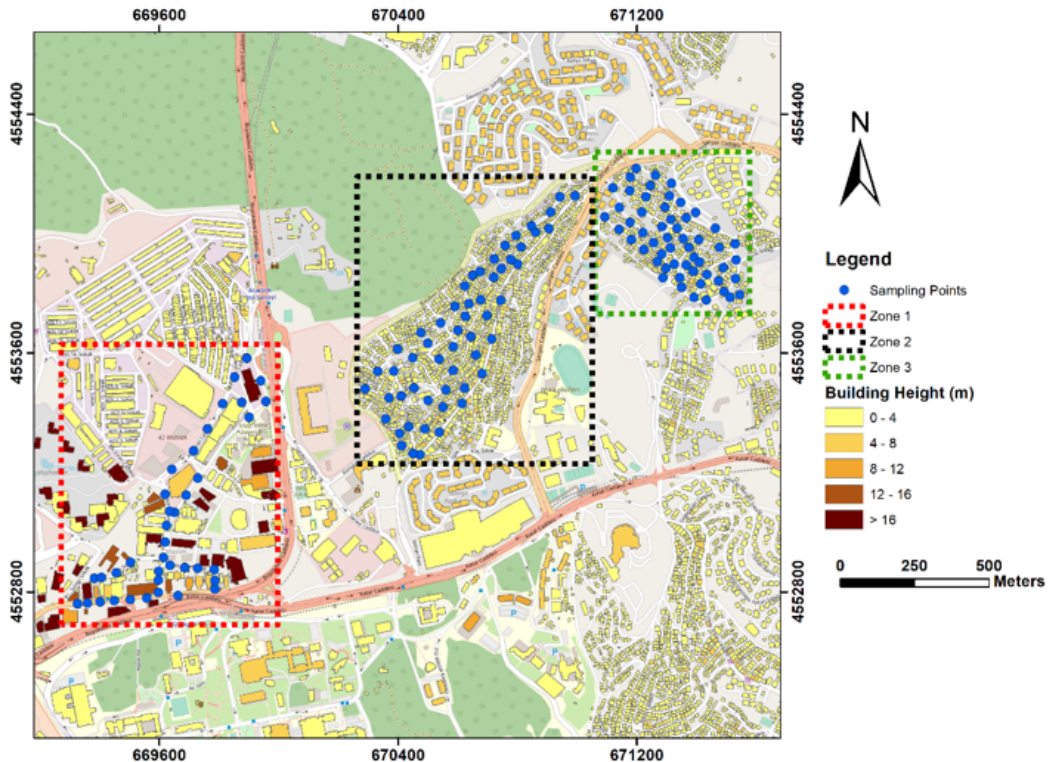


Figure 4

Building heights in the study area

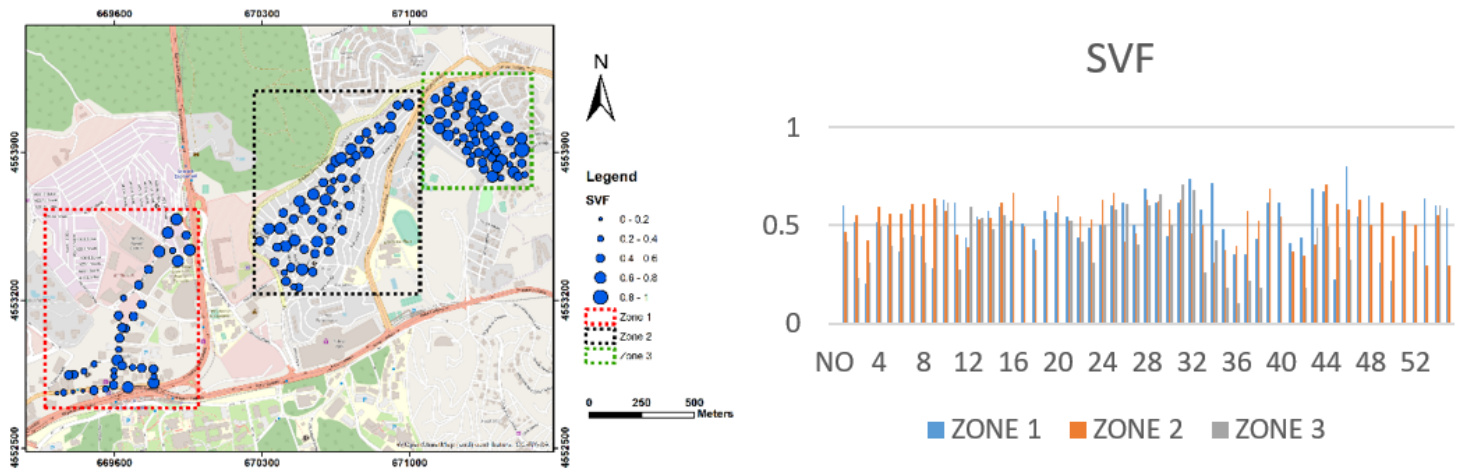


Figure 5

SVF values of zones in the study area.

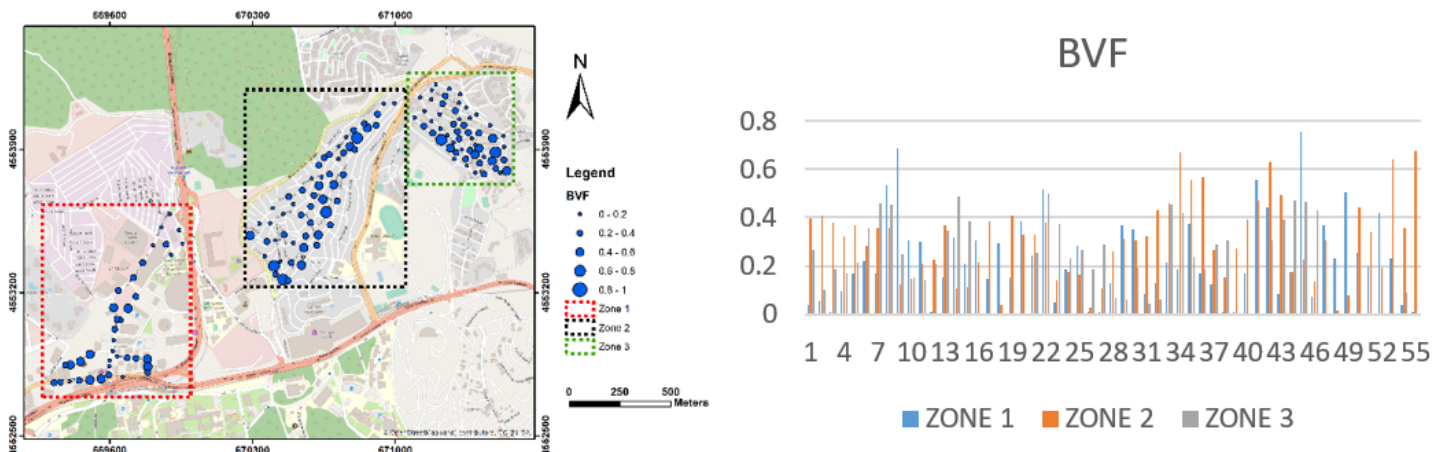


Figure 6

BVF values of zones in the study area

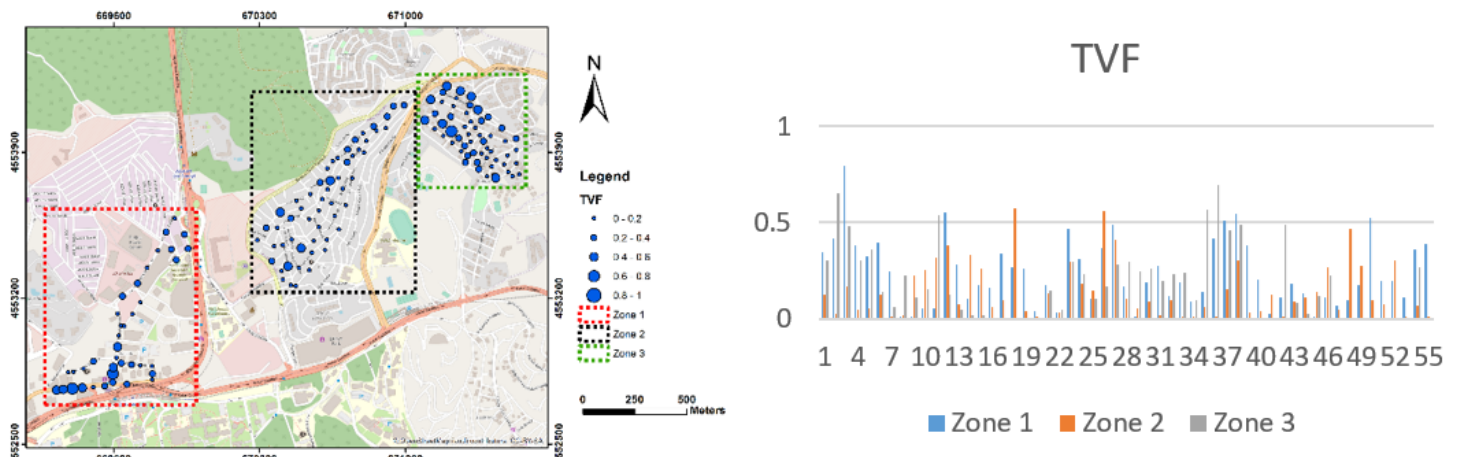


Figure 7

TVF values of zones in the study area

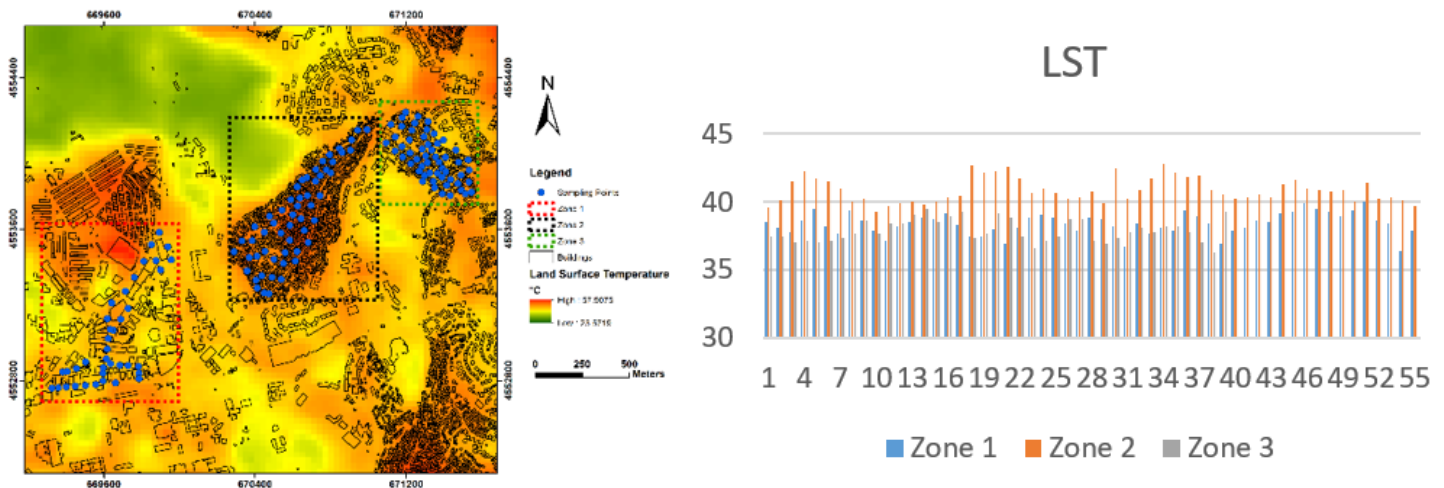


Figure 8

Surface temperature (LST) distribution of the study areas

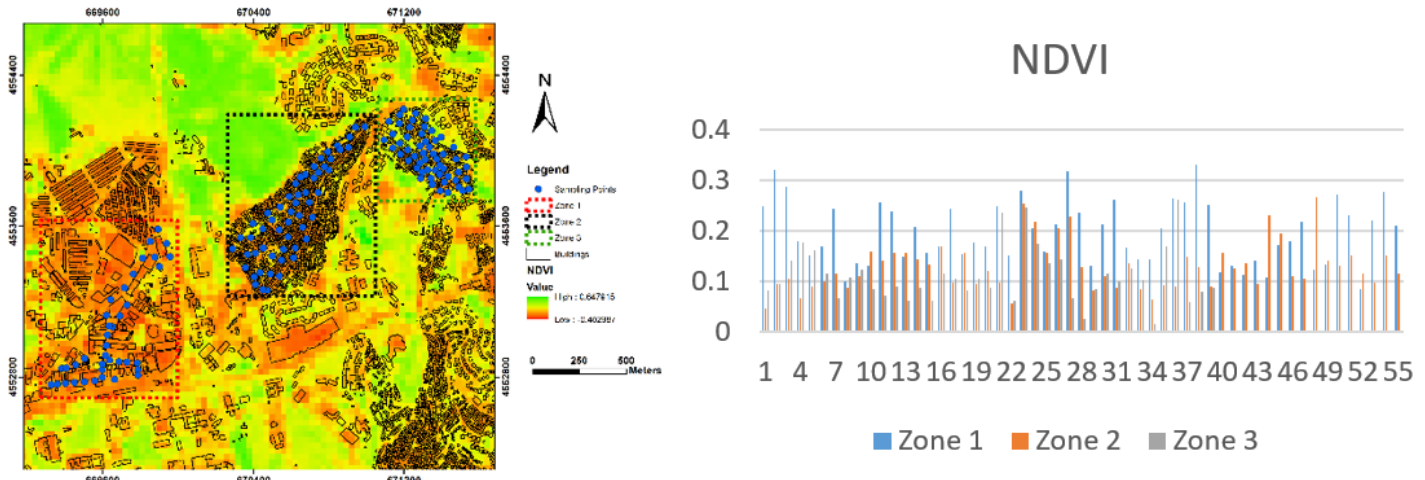


Figure 9

NDVI values of zones in the study area

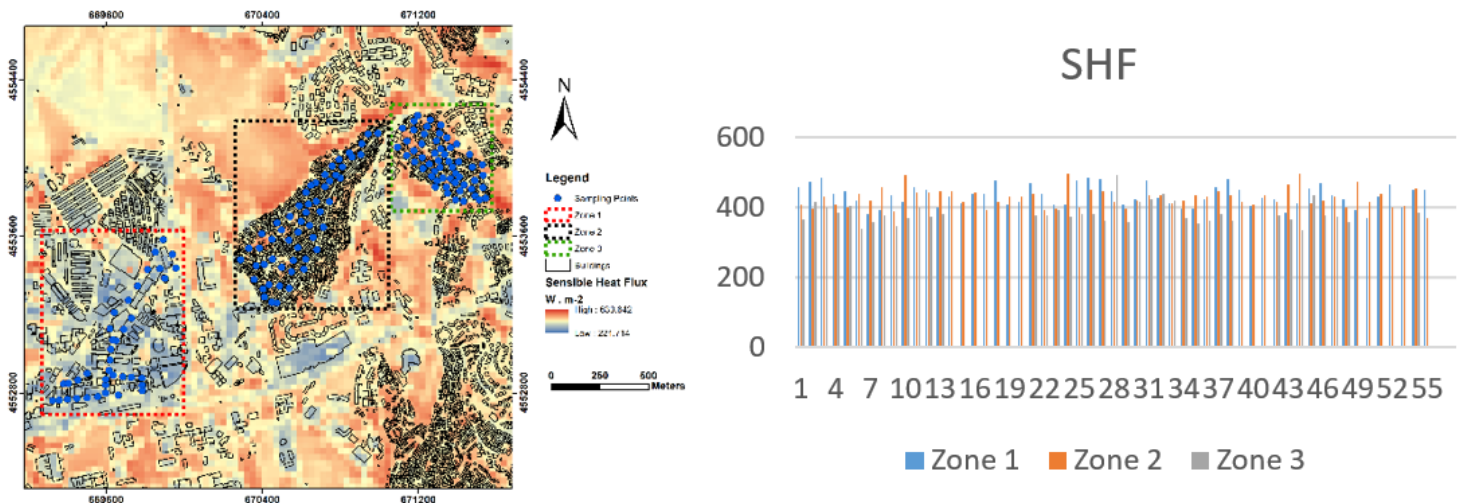


Figure 10

SHF values of zones in the study area

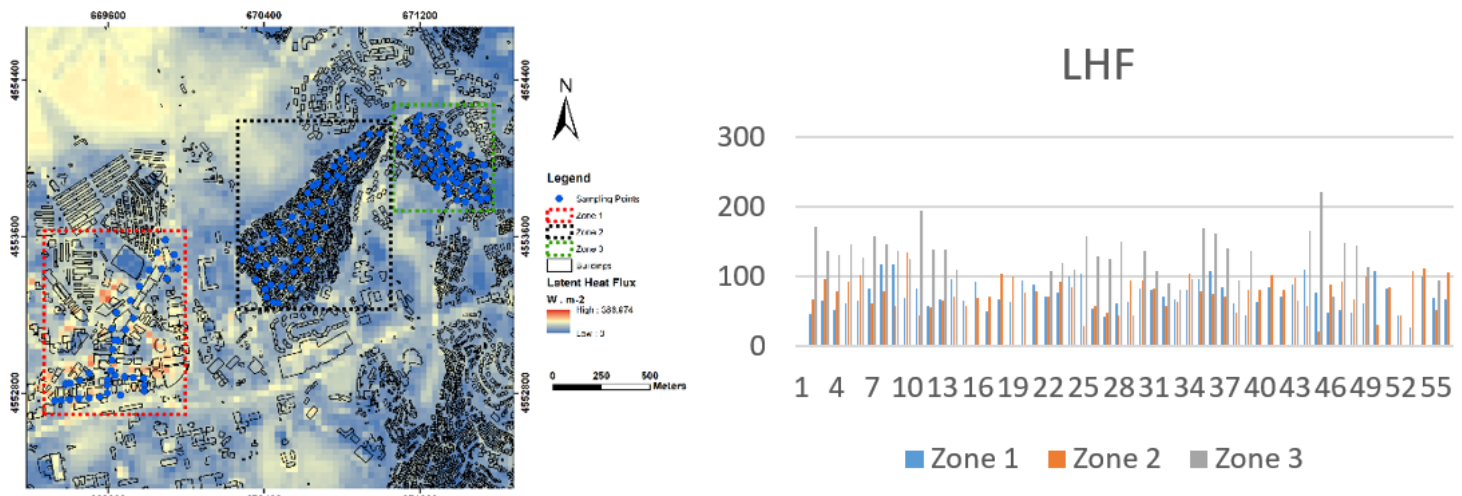


Figure 11

LHF values of zones in the study area

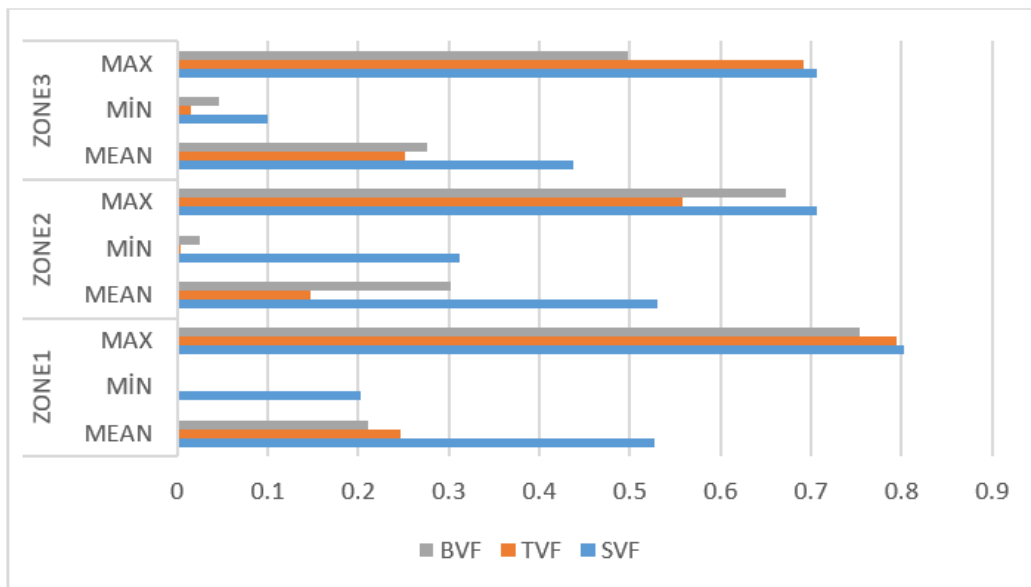


Figure 12

SVF-BVF-TVF values of study areas

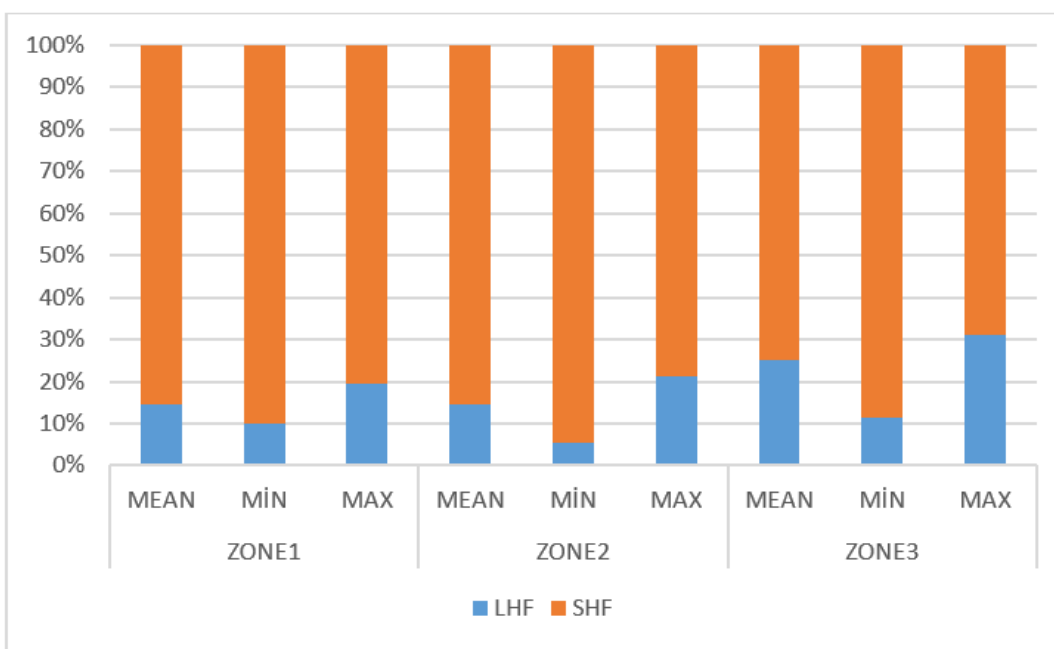


Figure 13

SHF-LHF values of study areas

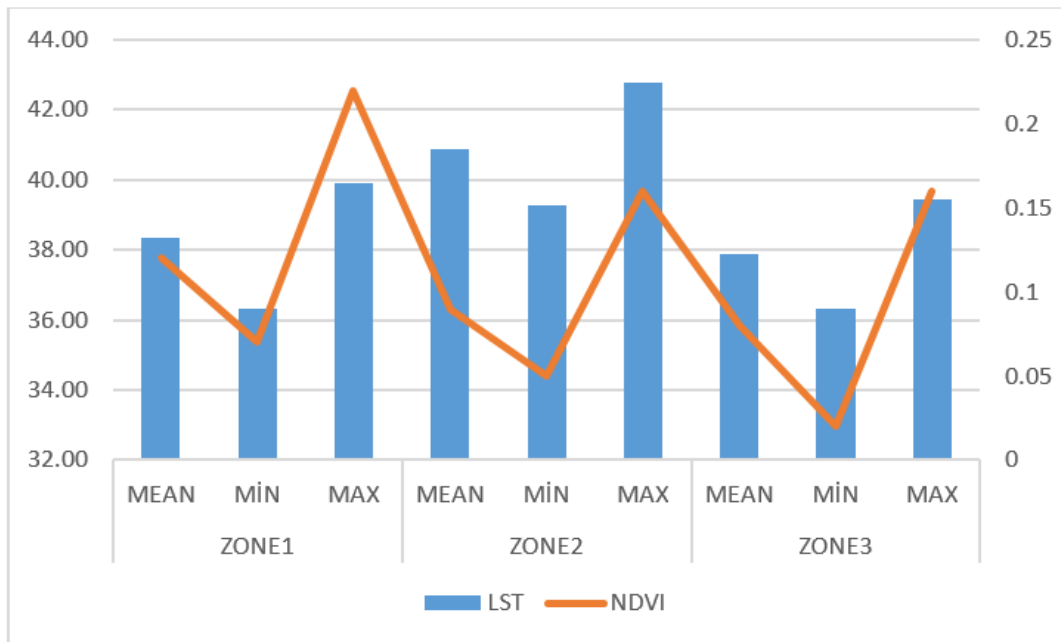


Figure 14

NDVI-LST relation in study areas

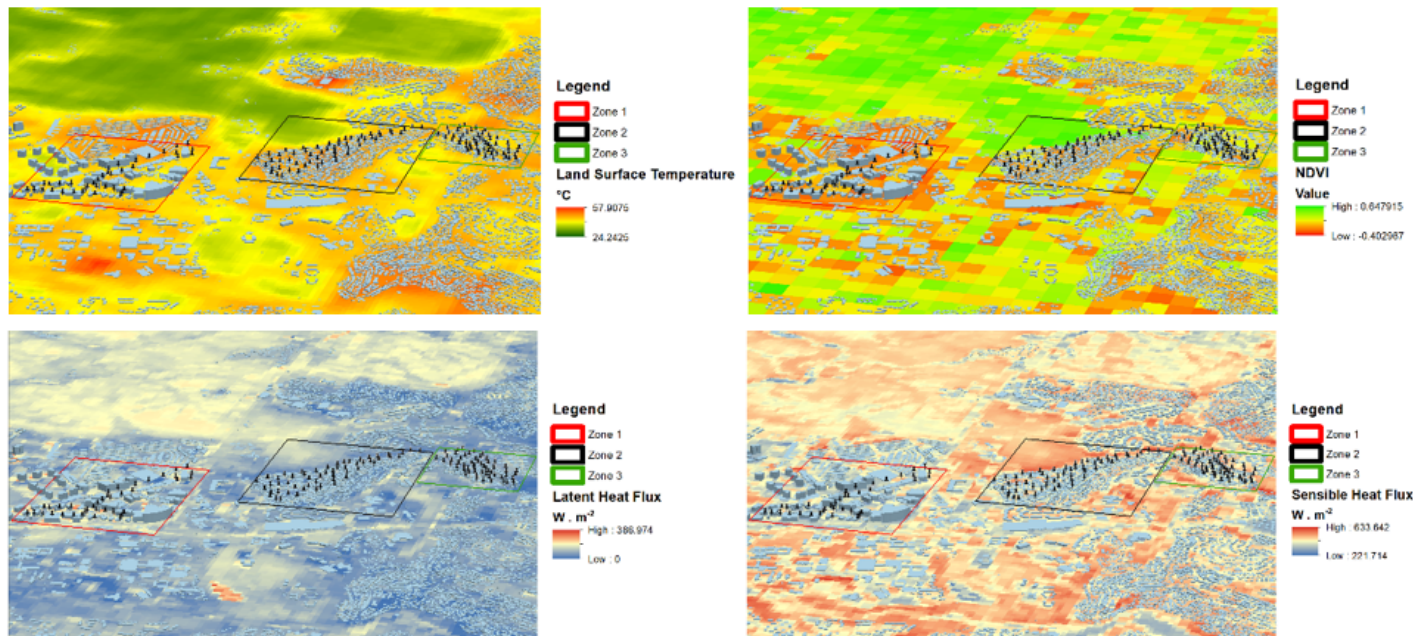


Figure 15

Display of LST, NDVI, LHF, and SHF values of study areas on 3D space